A multi-objective optimisation model for a general PEM fuel cell system

Sheila Mae C. Ang[a,b], Daniel J. L. Brett[a], Eric S. Fraga[*,a]

[a] *Department of Chemical Engineering, University College London (UCL), Torrington Place, London WC1E 7JE, United Kingdom*

[b] *Department of Chemical Engineering, University of the Philippines, Diliman, Quezon City 1101 Philippines*

Abstract

This paper presents an optimisation model for a general polymer electrolyte membrane (PEM) fuel cell system suitable for efficiency and size trade-offs investigation. Simulation of the model for a base case shows that for a given output power, a more efficient system is bigger and *vice versa*. Using the weighting method to perform a multi-objective optimisation, the Pareto sets were generated for different stack output powers. A Pareto set, presented as a plot of the optimal efficiency and area of the membrane electrode assembly (MEA), gives a quantitative description of the compromise between efficiency and size. Overall, our results indicate that, to make the most of the size-efficiency trade-off behaviour, the system must be operated at an efficiency of at least 40% but not more than 47%. Furthermore, the MEA area should be at least 3 cm^2 per Watt for the efficiency to be practically useful. Subject to the constraints imposed on the model, which are based on technical practicalities, a PEM fuel cell system such as the one presented in this work cannot operate at an efficiency above 54%. The results of this work, specifically the multi-objective model, will form a useful and practical basis for subsequent techno-economic studies for specific applications.

*Corresponding author, email: e.fraga@ucl.ac.uk, tel. +44(0)20 7679 3817, fax +44(0)20 7383 2348

Key words: fuel cell; multi-objective optimisation; design; modelling

1. Introduction

A fuel cell is an electrochemical engine that converts chemical potential into electric power. This technology is a promising power source for both mobile and stationary applications [1] as concern over depleting stocks of natural resources grows and awareness of environmental problems caused by burning of fossil fuels intensifies. Amongst the attractive benefits are high efficiency, low greenhouse gas emissions and quiet operation [2].

Several types of fuel cells are at present under development. The classification is primarily by the kind of electrolyte [1], which determines the chemical reaction that takes place in the cell, the catalyst required, the operating temperature range, and the fuel required. For certain applications, polymer electrolyte membrane (PEM) fuel cells are favored over other types of fuel cells for the following reasons: their high power density means they are lighter and smaller compared to other fuel cells, low operating temperature allows fast start-up and immediate response in power demand, and use of a solid polymer simplifies assembly and handling [1].

Fuel cells are inherently more efficient than a combustion engine of comparable size. The maximum efficiency of an internal combustion engine is limited by the Carnot efficiency [3]. For instance, the highest achievable efficiency of internal combustion engines having output power below 250 kW is 35%. Unlike a combustion engine, a fuel cell does not need to achieve a large temperature differential to achieve the same efficiency because its efficiency is determined by the Gibbs free energy [4]. The fuel cell system efficiency requirement for both stationary and transportation applications is at least 40% [5, 6].

Significant effort has been exerted in recent years to achieve optimal PEM fuel cell system design. Even though most of these studies make significant contributions to the expanding PEM fuel cell literature (e.g. formulation of PEM fuel cell models with different levels of complexity and development of various optimisation techniques), most of them are limited to a single design objective. Many studies have optimised the performance [7, 8, 9, 10, 11, 12, 13, 14, 15], whilst some have considered the cost [16], the durability [17], and the emission [18] as objectives for the design. Moreover, some of the papers have performed single-objective optimisation for a specific part of the PEM fuel cell system such as the membrane electrode assembly (MEA) [19], the electrode [20], the bipolar plate and diffusion layer [21], the cathode and air distributor [22], and the catalyst layer [23, 24]. However, the results of these studies might be misleading because the interaction or coupling between the multiple objectives has not been considered [6]. In addition, the potentially conflicting nature of the objectives makes the determination of the optimal solution more challenging.

There are a few papers in the literature that have dealt with multi-objective optimisation. Barbir and Gomez [5] analysed the cost and performance of PEM fuel cells at different load profiles and design and cost scenarios. Their efficiency model was based on a linear polarisation curve. Similar objectives were considered by Xue and Dong [3] in their multi-objective optimisation of the 120 kW Ballard Mark V Transit Bus fuel cell system with the stack active intersection area and the air stoichiometric ratio as the design variables. Frangopoulos and Nakos [25] investigated the Ballard Mark V PEM fuel cell stack consisting of 35 5 kW cells for a merchant ship application. The system efficiency, power density and present worth cost were the design objectives, whilst the current density and temperature were the design variables. In their study, the interaction between the objectives was not considered; they optimised each objective individually. Also, for each objective, one of the two design variables was

treated as a parameter. This resulted in a one-variable, single-objective optimisation problem, which was then solved at different values of the parameter. Na and Gou [6] optimised the efficiency and cost of a 50 kW PEM fuel cell system for transportation, using the system pressure, the hydrogen and air stoichiometric ratios, and the current density as the design variables. The Pareto set that they obtained using MATLAB's `fminimax` function, however, was influenced by the choice of the initial values of the design variables used in the solver, indicating the non-globality of the solution.

The trade-off between efficiency and size is inherent in the design of PEM fuel cell systems. These two objectives are both related to economics. Fuel consumption, hence operating cost, is directly determined by the efficiency. On the other hand, the bulk of the capital cost is contributed by the size of the MEA. The costs of the other components, such as the bipolar plates and auxiliaries (humidifiers, air compressor, and water coolant) which add up to the capital cost are strongly correlated with the variation in the area of the MEA [26]. However, the compromise between the capital investment and operating cost is not the only motivation for the trade-off investigation between size and efficiency. In the current consumer demographic, size and portability, for instance, may be the deciding factors for mobile users. On the other hand, other users may value operating costs more than portability.

This article presents a model suitable for multi-objective optimisation which allows us to investigate the efficiency and size trade-offs involved in the design of PEM fuel cell systems. The objective is to determine a set of trade-off optimal solutions, called the non-dominated or Pareto set, that maximises the efficiency and minimises the size of the system with respect to the current density, the cell voltage, the system pressure, the hydrogen and air stoichiometric ratios, and the relative humidities of fuel and air. To date, papers on multi-objective optimisation of PEM fuel cells have considered models that are specific to the application described in the paper [3, 6, 25, 27]. Our model is

more general and, thus, will be suitable for a wide range of applications. Furthermore, the model considers the multi-phase existence of water in the channels, thus capturing the fuel cell phenomena more thoroughly.

This paper is arranged as follows: Section 2 presents a general PEM fuel cell system and the model. Section 3 describes the multi-objective optimisation problem formulation based on this model and the solution approach taken. Section 4 presents results for a case study involving different output powers and highlights the important results from the analyses of the generated Pareto sets for the efficiency and size trade-offs.

2. A model for a general PEM fuel cell system

The major components of a general hydrogen-air PEM fuel cell system are shown in Figure 1. The system includes a stack and the auxilliaries needed to operate the fuel cell. In this paper, a single-cell stack has been considered. Once the total active MEA area is known, the number of cells can be determined given the active area of a single cell. This study does not consider components such as a reformer or fuel processer, the power electronics, controllers, and any auxilliary power sources. At the anode side, pure pressurised hydrogen is fed; at the cathode side, there is an air supply system which includes a compressor. A humidifier is located on both sides for stack water management. A coolant regulates the operating temperature of the cell. This study assumes uniform temperature and pressure throughout the stack. The amount of power produced depends on several factors including the cell size, operating temperature and pressure, and flow rates and humidity of the gases supplied to the cell.

Multi-objective optimisation requires the evaluation of a large number of design alternatives with correspondingly high computational requirements. At present the use of a complex model is not practical for this purpose. We propose a simple and fast model for multi-objective optimisation. The model has an acceptable accuracy and is complex

enough to differentiate between alternative designs, whilst being simple enough to allow for repeated calculations during optimisation.

In this work, the model is mainly based on an established, and well validated, principles presented by Nguyen and White [28]. In addition to the assumptions listed in Ref. [28], our model does not account for the spatial variations of the variables in the flow channels. Furthermore, we modified the water balance of Nguyen and White to address its non-validity in the event of no liquid water in the channels [29], and its inconsistency when both liquid and vapour phases of water are present, i.e. their model does not guarantee the equality between the partial pressure and vapour pressure of water at equilibrium. Also, the expression for the concentration of water in the membrane was taken from Hinatsu *et al.* [30], as appropriate for the temperature considered in this study.

2.1. Mass balances

For a given current density, the respective hydrogen and oxygen mass balances are

$$M_{\mathrm{H_2,in}} = M_{\mathrm{H_2}} + \frac{AI}{2F} \tag{1}$$

$$M_{\mathrm{O_2,in}} = M_{\mathrm{O_2}} + \frac{AI}{4F} \tag{2}$$

The second term on the right of equations 1 and 2 are the consumption of hydrogen and oxygen, respectively.

Nitrogen does not participate in the reaction, thus, the incoming flow rate is equal to the outgoing flow rate.

$$M_{\mathrm{N_2,in}} = M_{\mathrm{N_2}} \tag{3}$$

The flow rates of water in the channels and the presence of liquid and vapour phases are affected by the following factors: the production of water at the cathode by the

electrochemical reaction, the transport of water from the anode to the cathode via electro-osmosis or drag, the back diffusion of water from the cathode to the anode, and the condensation and evapouration of water [28, 29, 31, 32].

The water balance in the anode channel is

$$M^{\mathrm{v}}_{\mathrm{w,a,in}} = M^{\mathrm{v}}_{\mathrm{w,a}} + M^{\mathrm{l}}_{\mathrm{w,a}} + \frac{A\alpha I}{F} \tag{4}$$

where α is the net water molecules per proton flux ratio. This equation states that the water vapour going into the anode channel either leaves as vapour or condensed liquid water or migrates across the membrane to the cathode channel. The fraction of liquid water, f_{a}, and the water vapour-liquid equilibrium in the anode channel are described by the following equations:

$$f_{\mathrm{a}} = \frac{M^{\mathrm{l}}_{\mathrm{w,a}}}{M^{\mathrm{v}}_{\mathrm{w,a}} + M^{\mathrm{l}}_{\mathrm{w,a}}} \tag{5}$$

$$0 = f_{\mathrm{a}} \left[\frac{M^{\mathrm{v}}_{\mathrm{w,a}}}{M^{\mathrm{v}}_{\mathrm{w,a}} + M_{\mathrm{H_2}}} P - P^{\mathrm{sat}}_{\mathrm{w}} \right] \tag{6}$$

where $f_{\mathrm{a}} \in [0, 1]$. If both liquid and vapour phases of water are present in the anode channel, i.e. $f_{\mathrm{a}} \neq 0$, the expression inside the bracket of equation 6, representing the vapour-liquid equilibrium condition, is zero. In this case, Raoult's Law describes the flow rate of water vapour going out of the anode channel, $M^{\mathrm{v}}_{\mathrm{w,a}}$. The flow rate of condensed liquid water going out of the anode channel, $M^{\mathrm{l}}_{\mathrm{w,a}}$, can be computed from equation 4. Conversely, if liquid water is not present in the anode channel, i.e. $f_{\mathrm{a}} = 0$, equilibrium between liquid and vapour phases of water does not exist. In this case, $M^{\mathrm{l}}_{\mathrm{w,a}} = 0$ and $M^{\mathrm{v}}_{\mathrm{w,a}}$ can be calculated from equation 4.

Similarly, the water balance in the cathode channel can be expressed as

$$M^{\mathrm{v}}_{\mathrm{w,c,in}} = M^{\mathrm{v}}_{\mathrm{w,c}} + M^{\mathrm{l}}_{\mathrm{w,c}} - \frac{A\alpha I}{F} - \frac{AI}{2F} \tag{7}$$

The terms on the right of equation 7 are the flow rates of water vapour and condensed liquid water going out of the cathode channel, the water vapour that migrated from the anode to the cathode channel, and the water generated at the cathode by the electrochemical reaction, respectively. The fraction of liquid water, f_{c}, and the water vapour-liquid equilibrium in the cathode channel are given by

$$f_{\mathrm{c}} = \frac{M^{\mathrm{l}}_{\mathrm{w,c}}}{M^{\mathrm{v}}_{\mathrm{w,c}} + M^{\mathrm{l}}_{\mathrm{w,c}}} \tag{8}$$

$$0 = f_{\mathrm{c}} \left[\frac{M^{\mathrm{v}}_{\mathrm{w,c}}}{M^{\mathrm{v}}_{\mathrm{w,c}} + M_{\mathrm{N_2}} + M_{\mathrm{O_2}}} P - P^{\mathrm{sat}}_{\mathrm{w}} \right] \tag{9}$$

where $f_{\mathrm{c}} \in [0, 1]$. The same reasoning given for equations 4 - 6 applies to equations 7 - 9.

The hydrogen and air flow rates going into the channels are determined by their respective stoichiometric ratios,

$$M_{\mathrm{H_2,in}} = \lambda_{\mathrm{H_2}} \frac{IA}{2F} \tag{10}$$

$$M_{\mathrm{O_2,in}} = \lambda_{\mathrm{air}} \frac{IA}{4F} \tag{11}$$

The water vapour flow rate going into the anode channel can be computed from the relative humidity of the hydrogen fuel,

$$M^{\mathrm{v}}_{\mathrm{w,a,in}} = \frac{y_{\mathrm{w,a,in}}}{1 - y_{\mathrm{w,a,in}}} M_{\mathrm{H_2,in}} \tag{12}$$

$$y_{\mathrm{w,a,in}} = RH_{\mathrm{fuel}} \frac{P^{\mathrm{sat}}_{\mathrm{w}}}{P} \tag{13}$$

where $y_{\mathrm{w,a,in}}$ is the mole fraction of water vapour going into the anode and $P^{\mathrm{sat}}_{\mathrm{w}}$ is the saturation pressure.

Similarly, we can describe the water vapour flow rate going into the cathode channel:

$$M^{\mathrm{v}}_{\mathrm{w,c,in}} = \frac{y_{\mathrm{w,c,in}}}{1 - y_{\mathrm{w,c,in}}} \left(M_{\mathrm{O_2,in}} + M_{\mathrm{N_2,in}}\right) \tag{14}$$

$$y_{\mathrm{w,c,in}} = RH_{\mathrm{air}} \frac{P^{\mathrm{sat}}_{\mathrm{w}}}{P} \tag{15}$$

2.2. Electrochemistry

The effective cell voltage can be expressed as the difference between the thermodynamically reversible cell voltage and the losses due to overpotential,

$$V = V_{\mathrm{oc}} + \frac{R\left(273+T\right)}{2F} \ln\left(\frac{P_{\mathrm{H_2}} P^{0.5}_{\mathrm{O_2}}}{P_{\mathrm{H_2O}}}\right) - \frac{R\left(273+T\right)}{0.5F} \ln\left(\frac{I}{I_0 P_{\mathrm{O_2}}}\right) - \frac{I t_{\mathrm{m}}}{\sigma_{\mathrm{m}}} - \beta I^{\mathrm{k}} \ln\left(\frac{I_{\mathrm{L}}}{I_{\mathrm{L}} - I}\right) \tag{16}$$

where V_{oc} is the open-circuit potential, I_0 is the exchange current density, βI^{k} is the amplification term associated with the total mass transport overpotential, expressed in potential units [33] , and I_{L} is the limiting current density. The first two terms on the right of equation 16 represent the thermodynamic reversible voltage based on the Nernst equation [29]. The third term is the activation overpotential [28], which is the voltage loss due to the rate of reactions on the surface of the electrodes. This assumes that the activation overpotential is mainly located at the cathode. The fourth term is the ohmic overpotential [28], which is the voltage drop due to the resistance to the flow of protons in the electrolyte. The last term is the overall concentration overpotential [33], which is the voltage loss due to the mass trasport limitation .

2.3. System efficiency

One of the key properties of a fuel cell, used to evaluate its performance, is the efficiency. The efficiency of the system is defined by

$$\eta = \frac{W_{\mathrm{stack}} - W_{\mathrm{prs}}}{W_{\mathrm{fuel}}} \tag{17}$$

where W_{stack} is the output power of the stack, W_{prs} is the parasitic power and W_{fuel} is the power inherent in the fuel used:

$$W_{\text{stack}} = n_{\text{cell}} AIV \tag{18}$$

$$W_{\text{prs}} = W_{\text{comp}} + W_{\text{others}} \tag{19}$$

$$W_{\text{fuel}} = \lambda_{\text{H}_2} n_{\text{cell}} \frac{IA}{2F} \text{LHV} \tag{20}$$

$$W_{\text{comp}} = \frac{c_{\text{p}} T_{\text{e}}}{\eta_{\text{c}} \eta_{\text{mt}}} \left[\left(\frac{P}{P_{\text{in}}} \right)^{0.286} - 1 \right] m_{\text{air}} \tag{21}$$

$$m_{\text{air}} = 3.57 \times 10^{-7} \lambda_{\text{air}} n_{\text{cell}} IA \tag{22}$$

$$W_{\text{others}} = 0.05 W_{\text{stack}} \tag{23}$$

In this paper, $n_{\text{cell}} = 1$, thus A represents the total active MEA area. Equations 18, 19, 21 and 22 were taken from Pei *et al.* [34]. The parasitic power is composed of the power consumption of the compressor, W_{comp}, and the other power losses, W_{others}. Pei *et al.* [34] assumed W_{others} to be equal to 2 kW based on a stack output power of 62.5 kW. Instead, we set W_{others} to 5% of the nominal stack output power for the equations above to be applicable at different stack output powers. Also, the compressor and motor efficiencies vary with the size of the compressor and the fraction of full load at which it is operated at. However, it is assumed that the compressor and motor efficiencies are constant, similar to the approach adopted by others [6, 34].

Table 1 presents the expressions for the physical parameters used in the model, whilst Table 2 gives the values of the constant parameters.

2.4. Model validation

The model was evaluated for a base case corresponding to a stack having a MEA total active area of 25×10^4 cm^2 and an operating temperature of 80°C. Pure hydrogen at 100% relative humidity and air at 50% relative humidity are supplied to the anode and

cathode channels, respectively. The hydrogen stoichiometric ratio is 1.25 (i.e. hydrogen utilisation rate of 80%), whilst the air stoichiometric ratio is 2.

Figures 2(a)-(c) show the effects of operating pressure and current density on polarisation, system efficiency, and power density curves, respectively. With respect to the current density, the polarisation curve, which is commonly used as a measure of the performance of fuel cell systems, is in direct correlation with the system efficiency. The voltage, and hence the efficiency, decreases with increasing current density due to the combined irreversibility contributions of activation, ohmic and concentration overpotentials. The power density, on the other hand, increases with increasing current density and displays a maximum at a particular value of the current density. The polarisation curves also show that gains in voltage result when pressure is increased. However, the pressure has no significant effect on the system efficiency because the increase in cell potential is offset by the increase in parasitic power with increasing pressure. Furthermore, at high current densities, the power density increases with increasing pressure. These results are in agreement with the conclusions drawn by a large section of the literature [35, 36, 37, 38, 39, 40, 41].

The solution of the base case suggests that the efficiency and size are conflicting objectives. To achieve high efficiency, the system must be operated at low current density. At low current density the power density is also low, which means a larger system per unit of power. Conversely, for the same output power, a small system requires high power density, which demands high current density, resulting in a lower efficiency. The systematic and detailed investigation of the trade-offs between the efficiency and size is the focus of the succeeding sections.

3. Multi-objective optimisation

The model presented in the previous section has been shown to behave as expected for a base case. The simulation of the model for a base case reveals that for a given output power, a more efficient fuel cell is bigger and *vice versa*. We now wish to use this model within an optimisation-based design framework. The aim is to identify the efficiency and size trade-offs involved in the design of PEM fuel cell system for any given output power. The determination of a set of optimal solutions that represent the compromise between the objectives, called the non-dominated or Pareto set, requires a multi-objective optimisation technique.

There is a large variety of techniques for solving multi-objective optimisation problems [42]. In this paper, the weighting method is used to approximate the Pareto set. This method transforms the multi-objective optimisation problem into a single-objective optimisation problem by associating each objective function with a weighting coefficient and then minimising the weighted sum of the objectives. This can be expressed mathematically as

$$\min z = \sum_{i=1}^{N} \omega_i z_i \tag{24}$$

where $\omega_i \in [0, 1]$ and $\sum_{i=1}^{N} \omega_i = 1$. In equation 24, z is the weighted sum of the objectives, z_i is a single-objective and ω_i is a weighting factor. The solution of equation 24 produces a single result that is as good as the selection of the weights [43]. A Pareto set can be generated by evaluating a series of single-objective optimisation problems at different values of the weighting factor to avoid having to, *a priori*, select a particular weighting between objectives.

The PEM fuel cell system efficiency-size multi-objective optimisation problem is for-

mulated using the weighting method as

$$\min_{I,P,\lambda_{\mathrm{H}_2},\lambda_{\mathrm{air}},RH_{\mathrm{fuel}},RH_{\mathrm{air}}} z = -\omega\eta + (1-\omega)\,A \tag{25}$$

subject to:

$$0.11\,\mathrm{A\ cm^{-2}} \leq I \leq 1.3\,\mathrm{A\ cm^{-2}}$$

$$1.2\,\mathrm{atm} \leq P \leq 5\,\mathrm{atm}$$

$$1.1 \leq \lambda_{\mathrm{fuel}} \leq 10$$

$$1.1 \leq \lambda_{\mathrm{air}} \leq 10$$

$$0.5 \leq RH_{\mathrm{fuel}} \leq 1$$

$$0.5 \leq RH_{\mathrm{air}} \leq 1$$

The system efficiency, η, is given by equation 17, whereas the system size is represented by the total active area of the MEA, A. The size of the other components such as the bipolar plates and auxiliaries (humidifiers, air compressor, and water coolant) are directly correlated with the variation in the area of the MEA. A single-cell fuel cell stack has been considered. Once the total active area is known, the number of cells can be determined given the active area of a single cell. Although a fuel cell's performance will be affected by the temperature, in this study the temperature is fixed at 80°C. It is difficult to derive a reliable analytical expression for the exchange current density, I_0, as a function of the temperature, since it depends on the specifics of the catalyst used. The lower bound on the pressure is 1.2 atm because the compressor cannot provide a pressure below atmospheric (i.e. the system pressure is always higher than the atmospheric pressure) [6]. The lower bound on the hydrogen and air stoichiometric ratios should be higher than the minimum limit to prevent depletion [6]. With regard to the relative humidity, when using air as the oxidant it is a common practice to use at

least 50% relative humidity. Using the same set of objective function and constraints, the Pareto set is obtained at different stack output powers, namely 1, 25, 50, 75 and 100 kW.

In equation 25, $\omega \in [0, 1]$ represents the weighting factor. The negative sign in front of the efficiency objective indicates a maximisation problem. The extreme points $\omega = 0$ and $\omega = 1$ represent the single-objective optimisation problems where the size and the efficiency are minimised and maximised, respectively. Solving the optimisation problem for any $\omega \in (0, 1)$ will generate solutions between these two extremes where the two objectives will be considered simultaneously. The value of ω will determine the relative importance of each objective. For example, at $\omega = 0.25$**,** the size is of higher importance than the efficiency. The reverse is true at $\omega = 0.75$, in which more weight is given to the efficiency than size. However, assigning equal weights to the objectives does not necessarily mean giving equal importance to the objectives. Furthermore, as the relative weights matter in this technique, the objectives were scaled to have comparable values. In addition, since the problem involves both maximisation and minimisation, the solver may be ineffective in searching the region at which the value of the weighted sum of the objectives is zero. This can be overcome by translating the problem (i.e. adding an appropriate constant to equation 25) such that the values of the weighted sum of the objectives are either positive or negative for all ω's.

The optimisation model was written in the GAMS [44] modelling language and was solved using LINDOGlobal. LINDOGlobal employs branch-and-cut method to break a nonlinear programming (NLP) model down into a list of subproblems [45]. A discussion of the branch-and-cut method is given in [46]. For a given weighting factor, ω, an optimisation run usually converges to a solution with a relative tolerance of 0.01% after approximately 120 seconds on a desktop computer with a 2.66 GHz Intel Core Duo CPU and with 2GB RAM.

4. Results and discussion

Figure 3 gives the trade-off solutions for a stack output power of 50 kW. The efficiency and the MEA area are plotted on the two axes and the curve consists of a set of designs that are all optimal in a Pareto sense. For comparison, the base case solution at stack output power of 50 kW and pressure of 2 atm (referred later as base case) is given in the first row of Table 3. The highest point (top right) in Figure 3 represents the optimal solution at $\omega = 1$, which corresponds to the single objective optimisation problem of maximising the efficiency of the system without taking the size into account. This solution is 20% more efficient but 112% bigger in size relative to the base case. This solution requires operation at a lower current density (thus, a higher voltage), at a higher pressure, and with lower hydrogen and air stoichiometric ratios with respect to the base case. As a consequence of the higher efficiency, this solution has a lower fuel consumption. However, the parasitic loss is higher due to the increase in the pressure. Conversely, the lowest point (bottom left) in the curve corresponds to the optimal solution at $\omega = 0$, which is the minimisation of the size regardless of the efficiency. This solution represents a design that is 42% smaller in size but 44% less efficient than the base case. In comparison with the base case, this design has a higher operating current density (thus, a lower voltage), operates at a higher pressure, and with lower hydrogen and air stoichiometric ratios. This design has higher power consumption and parasitic loss. From the results, it can be concluded that the efficiency and size of the system must be optimised simultaneously. If only the efficiency is maximised, the outcome is a possibly impractically large system. On the other hand, optimising for size results in a system almost four times smaller in size but efficiency that is less than desirable.

As shown in Figure 3, the base case is a dominated solution because it lies "inside" of

the Pareto set. In Figure 3, the points that correspond to $\omega = 0.60$ up to $\omega = 0.65$ have both a higher efficiency and a smaller size compared to the base case so they improve on both objectives.

The points at the far right of Figure 3 represent solutions in which the size of the system is compromised in favour of the efficiency. Moving down the curve, to the left, the size of the system is improved but the efficiency reduces. None of the points is essentially superior and the final design choice will depend on the factors specific to the application. For stationary applications, the size of the system can be traded for the efficiency. This is not the case, however, for mobile and transportation applications which require highly efficient and small systems. Furthermore, at the efficiency of approximately 47% and above, the slope of the curve is very steep. In this region large increases in the size of the system result in small gains in efficiency. For instance, 51% efficiency is better than 52% from an economic point of view. This is because approximately 6 m^2 (15%) additional MEA area is likely to be too much to justify the 1% increase in the efficiency. Conversely, at the efficiency of about 40% and below, the curve appears to be flat. This suggests that in this region, a small change in the size of the system leads to a large impact on the efficiency. An example from Figure 3 is a 5% efficiency jump from 25% to 30% will only require 0.20 m^2 (1.5%) increased in the MEA area. In this region, the average increase in the MEA area is roughly 0.20 m^2 for every 1% increase in the efficiency. Overall, to make the most of the trade-off behaviour in Figure 3, the PEM fuel cell system must be operated at an efficiency of at least 40%.

Table 3 gives the optimal values of the design variables for the representative solutions highlighted in Figure 3. The extreme points, $\omega = 1$ and $\omega = 0$ represent the single-objective optimisation solutions and, thus are not expected to follow the trend of how each variable behaves. In general, moving from a high efficiency, large size solution to a non-dominated, low efficiency, small size solution in the Pareto set involves increases

in the operating current density (thus, decreased cell voltage) and pressure. The optimal values of the hydrogen fuel and air relative humidity turn out to be 1 and 0.5, respectively, for all ω's. The optimal hydrogen stoichiometric ratio is 1.1 (i.e. hydrogen utilisation rate of 91%) for all ω's except at an extreme point. Finally, in moving along the Pareto set in the mentioned manner, the fuel consumption and parasitic loss increase.

Similar analyses were performed for different stack output powers, namely, 1, 25, 50, 75 and 100 kW. Figure 4(a) shows the comparison of the generated Pareto sets. In this figure, the MEA area per Watt is plotted against the efficiency for each stack output power. The Pareto sets are qualitatively similar in shape but differ in span. Also, the solutions of the single-objective efficiency maximisation at different stack output powers nearly completely converge with an efficiency of 54% and a MEA area of 10.5 cm^2 per Watt . On the other hand, the solutions of the single-objective size minimisation settled at an average MEA area of 2.8 cm^2 per Watt with increasing efficiency as stack output power increases. A region of interest is enlarged in Figure 4(b) to emphasise the difference in the solutions at different stack output power. It can be observed that for a particular value of the efficiency, increasing the stack output power eventually results to an increase in the MEA area required per Watt of power produced. For example, at an efficiency of 45%, the MEA area per Watt at stack output power of 75 kW and 100 kW are 3% and 7%, respectively, bigger relative to the MEA area per Watt at stack output power of 1, 25, and 50 kW.

Figures 5 and 6 show the optimal values of the design objectives and some of the design variables, respectively, plotted against the current density for different stack output powers. The solutions that are large in size and high in efficiency, forming the right branches of the Pareto sets in Figure 4(a), occur at low current density. Conversely, the left branches of the Pareto sets in Figure 4(a), containing the solutions that are small

in size and low in efficiency, occur at high current density. Overall, with respect to the current density, the MEA area, efficiency and voltage are decreasing, whilst the input power and parasitic power are increasing. Furthermore, the input power and parasitic power are increasing, whilst the voltage and air stoichiometric ratio are decreasing with increasing stack output power. Moreover, the single-objective size minimisation at the stack output power of 1 kW resulted to a solution with zero efficiency. In this particular solution, the power produced by the stack is all consumed by the system as the parasitic loss resulting in a zero net output power.

It can also be observed from Figure 6 that some of the bounds on the design variables were hit during optimisation, specifically the lower bound on the current density, the upper bound on the pressure, and the bounds on the hydrogen stoichiometric ratio. Lowering the bounds on the current density and hydrogen stoichiometric ratio are not useful because in an actual operation current density below 0.11 A/cm^2 and hydrogen stoichiometric ratio less than 1.1 are not practical. Comparison of Figure 6(b) with Figure 4(a) shows that the solutions that hit the upper bound on the pressure correspond to the region in Figure 4(a) where the branches of the Pareto sets appear to be separated. These solutions could have achieved smaller sizes and higher efficiency values if the bound on the pressure had allowed them to.

Consequently, the effect of increasing the upper bound on the pressure to 10 atm was investigated. Pressures higher than 5 atm are not usually used in actual operation. This upper bound was only considered, in this paper, for diagnostic purposes. In Figure 7, the solutions that previously hit the 5 atm upper bound on the pressure assumed higher values of pressure when the bound is relaxed. The resulting Pareto sets for different stack output powers are shown in Figure 8. As an illustration, for the stack output power of 100 kW at an efficiency of 45%, the size is reduced by 6.25% by using an upper bound on the pressure of 10 atm (MEA area of 45 m^2) instead of 5 atm (MEA area

of 48 m^2). Moreover, the Pareto sets for different stack output powers appear to be closer to each other when compared with Figure 4. The slight separation is due to the solutions still reaching the 10 atm upper bound on the pressure at high current density.

5. Conclusion

An optimisation model for a general PEM fuel cell system, suitable for use within a multi-objective framework, has been proposed. This model allows us to investigate the trade-offs between the efficiency and the size. The simulation of the model for a base case shows that for a given output power, a more efficient system is bigger and *vice versa*. The Pareto sets, generated for different output powers, represent a quantitative description of the trade-offs between efficiency and size. The results of this study illustrate the importance of formulating the problem as a multi-objective optimisation. Maximisation of the efficiency without taking the size into account will result to a possibly impractically large system. Conversely, a significantly small system but with very low efficiency will result if the only objective is size. Overall, the system must be operated at an efficiency of at least 40% but not more than 47% to make the most of the size-efficiency trade-off behaviour. Furthermore, the MEA area should be at least 3 cm^2 per Watt for the efficiency to be practically useful. Moreover, given the constraints of the model, which are based on technical practicalities, a PEM fuel cell system such as the one presented cannot reach an efficiency of more than 54%. Our work presents a way of determining the PEM fuel cell system optimal design such that for a particular application, a balance between efficiency and size is achieved. The results from this work can be further applied to techno-economic studies given a specific application.

Acknowledgements

The scholarship support provided by the Department of Science and Technology (Philippines) and the University of the Philippines to Sheila Ang is gratefully acknowledged. This work has been partially funded by the EPSRC Supergen programme to support Dr. Brett's fuel cell research.

References

[1] EG&G Technical Services, Inc., Fuel Cell Handbook, 7th Edition, U.S. Department of Energy, Morgantown, West Virginia, 2004.

[2] J. Larminie, A. Dicks, Fuel Cell Systems Explained, 2nd Edition, John Wiley & Sons, Japan, 2003.

[3] D. Xue, Z. Dong, Optimal fuel cell system design considering functional performance and production costs, Journal of Power Sources 76 (1) (1998) 69–80.

[4] C. Spiegel, PEM Fuel Cell Modeling and Simulation Using MATLAB, Elsevier Inc., 2008.

[5] F. Barbir, T. Gomez, Efficiency and economics of proton exchange membrane (PEM) fuel cells, International Journal of Hydrogen Energy 22 (10-11) (1997) 1027–1037.

[6] W. Na, B. Gou, The efficient and economic design of PEM fuel cell systems by multi-objective optimization, Journal of Power Sources 166 (2) (2007) 411–418.

[7] M. Al-Baghdadi, H. Al-Janabi, Parametric and optimization study of a PEM fuel cell performance using three-dimensional computational fluid dynamics model, Renewable Energy 32 (7) (2007) 1077–1101.

[8] A. M. Azmy, I. Erlich, Online optimal management of PEM fuel cells using neural networks, IEEE Transactions on Power Delivery 20 (2) (2005) 1051–1058.

[9] S. Chen, J. C. Ordonez, J. V. C. Vargas, J. E. F. Gardolinski, M. A. B. Gomes, Transient operation and shape optimization of a single PEM fuel cell, Journal of Power Sources 162 (1) (2006) 356–368.

[10] P. K. Das, X. G. Li, Z. S. Liu, Analytical approach to polymer electrolyte membrane fuel cell performance and optimization, Journal of Electroanalytical Chemistry 604 (2) (2007) 72–90.

[11] W. R. W. Daud, A. B. Mohamad, A. A. H. Kadhum, R. Chebbi, S. E. Iyuke, Performance optimisation of PEM fuel cell during MEA fabrication, Energy Conversion and Management 45 (20) (2004) 3239–3249.

[12] J. Godat, F. Marechal, Optimization of a fuel cell system using process integration techniques, Journal of Power Sources 118 (1-2) (2003) 411–423.

[13] A. J. J. Kadjo, P. Brault, A. Caillard, C. Coutanceau, J. P. Gamier, S. Martemianov, Improvement of proton exchange membrane fuel cell electrical performance by optimization of operating parameters and electrodes preparation, Journal of Power Sources 172 (2007) 613–622.

[14] G. Karimi, J. J. Baschuk, X. Li, Performance analysis and optimization of PEM fuel cell stacks using flow network approach, Journal of Power Sources 147 (1-2) (2005) 162–177.

[15] J. Wishart, Z. Dong, A. Secanell, Optimization of a PEM fuel cell system based on empirical data and a generalized electrochemical semi-empirical model, Journal of Power Sources 161 (2) (2006) 1041–1055.

[16] K. I. Chen, J. Winnick, V. I. Manousiouthakis, Global optimization of a simple mathematical model for a proton exchange membrane fuel cell, Computers & Chemical Engineering 30 (8) (2006) 1226–1234.

[17] R. Chandrasekaran, W. Bi, T. F. Fuller, Robust design of battery/fuel cell hybrid systems-methodology for surrogate models of Pt stability and mitigation through system controls, Journal of Power Sources 182 (2) (2008) 546–557.

[18] S. K. Kamarudin, W. R. W. Daud, A. M. Som, M. S. Takriff, A. W. Mohammad, Synthesis and optimization of a PEM fuel cell system via reactor-separation network (RSN), Journal of Power Sources 159 (2) (2006) 1194–1204.

[19] S. E. Iyuke, A. B. Mohamad, A. A. H. Kadhum, W. R. W. Daud, C. Rachid, Improved membrane and electrode assemblies for proton exchange membrane fuel cells, Journal of Power Sources 114 (2) (2003) 195–202.

[20] C. C. Boyer, R. G. Anthony, A. J. Appleby, Design equations for optimized PEM fuel cell electrodes, Journal of Applied Electrochemistry 30 (7) (2000) 777–786.

[21] S. A. Grigoriev, A. A. Kalinnikov, V. N. Fateev, A. A. Wragg, Numerical optimization of bipolar plates and gas diffusion layers for PEM fuel cells, Journal of Applied Electrochemistry 36 (9) (2006) 991–996.

[22] M. Grujicic, C. L. Zhao, K. M. Chittajallu, J. M. Ochterbeck, Cathode and interdigitated air distributor geometry optimization in polymer electrolyte membrane (PEM) fuel cells, Materials Science and Engineering B-Solid State Materials for Advanced Technology 108 (3) (2004) 241–252.

[23] R. M. Rao, R. Rengaswamy, Optimization study of an agglomerate model for platinum reduction and performance in PEM fuel cell cathode, Chemical Engineering Research & Design 84 (A10) (2006) 952–964.

[24] S. D. Yim, W. Y. Lee, Y. G. Yoon, Y. J. Sohn, G. G. Park, T. H. Yang, C. S. Kim, Optimization of bifunctional electrocatalyst for PEM unitized regenerative fuel cell, Electrochimica Acta 50 (2-3) (2004) 713–718.

[25] C. A. Frangopoulos, L. G. Nakos, Development of a model for thermoeconomic design and operation optimization of a PEM fuel cell system, Energy 31 (10-11) (2006) 1501–1519.

[26] A. J. Hung, Y. H. Chen, L. Y. Sung, C. C. Yu, Cost analysis of proton exchange membrane fuel cell systems, AICHE Journal 54 (7) (2008) 1798–1810.

[27] K. Subramanyan, U. M. Diwekar, A. Goyal, Multi-objective optimization for hybrid fuel cells power system under uncertainty, Journal of Power Sources 132 (1-2) (2004) 99–112.

[28] T. V. Nguyen, R. E. White, A water and heat management model for proton-exchange-membrane fuel-cells, Journal of the Electrochemical Society 140 (8) (1993) 2178–2186.

[29] J. Golbert, D. R. Lewin, Model-based control of fuel cells: (1) regulatory control, Journal of Power Sources 135 (1-2) (2004) 135–151.

[30] J. T. Hinatsu, M. Mizuhata, H. Takenaka, Water-uptake of perfluorosulfonic acid membranes from liquid water and water-vapor, Journal of the Electrochemical Society 141 (1994) 1493–1498.

[31] J. S. Yi, T. V. Nguyen, An along-the-channel model for proton exchange membrane fuel cells, Journal of the Electrochemical Society 145 (4) (1998) 1149–1159.

[32] S. H. Ge, B. L. Yi, A mathematical model for PEMFC in different flow modes, Journal of Power Sources 124 (1) (2003) 1–11.

[33] G. Squadrito, G. Maggio, E. Passalacqua, F. Lufrano, A. Patti, An empirical equation for polymer electrolyte fuel cell (PEFC) behaviour, Journal of Applied Electrochemistry 29 (12) (1999) 1449–1455.

[34] P. C. Pei, W. Yang, P. Li, Numerical prediction on an automotive fuel cell driving system, International Journal of Hydrogen Energy 31 (3) (2006) 361–369.

[35] F. Barbir, PEM Fuel Cells: Theory and Practice, Academic Press, 2005.

[36] J. Kim, S.-M. Lee, S. Srinivasan, C. E. Chamberlin, Modeling of proton exchange membrane fuel cell performance with an empirical equation, Journal of the Electrochemical Society 142 (1995) 2670–2674.

[37] L. Wang, A. Husar, T. H. Zhou, H. T. Liu, A parametric study of PEM fuel cell performances, International Journal of Hydrogen Energy 28 (11) (2003) 1263–1272.

[38] A. Kazim, P. Lund, Basic parametric study of a proton exchange membrane fuel cell, Proceedings of the Institution of Mechanical Engineers Part A - Journal of Power and Energy 220 (A8) (2006) 847–853.

[39] A. Mughal, X. Li, Experimental diagnostics of PEM fuel cells, International Journal of Environmental Studies 63 (4) (2006) 377–389.

[40] Q. G. Yan, H. Toghiani, H. Causey, Steady state and dynamic performance of proton exchange membrane fuel cells (PEMFCs) under various operating conditions and load changes, Journal of Power Sources 161 (1) (2006) 492–502.

[41] Y. Zhang, R. Pitchumani, Numerical studies on an air-breathing proton exchange membrane (PEM) fuel cell, International Journal of Heat and Mass Transfer 50 (23-24) (2007) 4698–4712.

[42] U. Diwekar, Introduction to Applied Optimization, New York : Springer, 2008.

[43] P. Ngatchou, A. Zarei, M. El-Sharkawi, Pareto multi objective optimization, Proceedings of the 13th International Conference on Intelligent Systems Application to Power Systems, 2005 (2005) 84–91.

[44] R. E. Rosenthal, GAMS - A User's Guide, GAMS Development Corporation, Washington, DC, USA (2008).

[45] Lindo Systems, Inc., LINDOGlobal.

[46] A. Lucena, J. Beasley, Branch and cut algorithms, in: J. E. Beasley (Ed.), Advances in linear and integer programming, Oxford University Press, Inc., Oxford, 1996, pp. 187–221.

[47] T. Springer, T. Zawodzinski, S. Gottesfeld, Polymer electrolyte fuel-cell model, Journal of the Electrochemical Society 138 (8) (1991) 2334–2342.

[48] T. Springer, T. Zawodzinski, S. Gottesfeld, Modeling water content effects in polymer electrolyte fuel cells. In Modelling of Batteries and Fuel Cells, vol. 91(10), Softbound Proceedings Series. White R , Verbrugge M , Stockel J (eds). The Electrochemical Society: Pennington, NJ; 209-223.

List of Tables

List of Figures

Table 1: Expressions for the physical parameters in the model

Description	Equation	Ref.
Activity of water in the anode channel	$a_{\mathrm{a}} = \frac{y_{\mathrm{w,a}} P}{P_{\mathrm{w}}^{\mathrm{sat}}} = \left(\frac{M_{\mathrm{w,a}}^{\mathrm{v}}}{M_{\mathrm{w,a}}^{\mathrm{v}} + M_{\mathrm{H_2}}} \right) \frac{P}{P_{\mathrm{w}}^{\mathrm{sat}}}$, $a_{\mathrm{a}} \in [0, 1]$	
Activity of water in the cathode channel	$a_{\mathrm{c}} = \frac{y_{\mathrm{w,c}} P}{P_{\mathrm{w}}^{\mathrm{sat}}} = \left(\frac{M_{\mathrm{w,c}}^{\mathrm{v}}}{M_{\mathrm{w,c}}^{\mathrm{v}} + M_{\mathrm{O_2}} + M_{\mathrm{N_2}}} \right) \frac{P}{P_{\mathrm{w}}^{\mathrm{sat}}}$, $a_{\mathrm{c}} \in [0, 1]$	
Concentration of water at the k interface of the membrane	$c_{\mathrm{w},k} = \frac{\rho_{\mathrm{m,dry}}}{M_{\mathrm{m,dry}}} (0.300 + 10.8 a_k - 16.0 a_k^2 + 14.1 a_k^3)$, $k = \mathrm{a}, \mathrm{c}$, $a_k \in [0, 1]$	[30]
Diffusion coefficient of water in the membrane	$D_{\mathrm{w}} = n_{\mathrm{d}} D_0 \exp\left[2416 \left(\frac{1}{303} - \frac{1}{273 + T} \right)\right]$	[28, 47, 48]
Electro-osmotic coefficient	$n_{\mathrm{d}} = 0.0049 + 2.024 a_{\mathrm{a}} - 4.53 a_{\mathrm{a}}^2 + 4.09 a_{\mathrm{a}}^3$, $a_{\mathrm{a}} \in [0, 1]$	[28, 47, 48]
Membrane conductivity	$\sigma_{\mathrm{m}} = \left(0.00514 \frac{M_{\mathrm{m,dry}}}{\rho_{\mathrm{m,dry}}} c_{\mathrm{m}} - 0.00326 \right) \cdot \exp\left[1268 \left(\frac{1}{303} - \frac{1}{273 + T} \right)\right]$	[47]
Net water molecules per proton flux ratio	$\alpha = n_{\mathrm{d}} - \frac{F}{I} D_{\mathrm{w}} \frac{(c_{\mathrm{w,c}} - c_{\mathrm{w,a}})}{t_{\mathrm{m}}}$	[47]
Partial pressure of component i	$P_{\mathrm{i}} = \frac{M_{\mathrm{i}}}{\sum M_{\mathrm{j}}} P$, anode: i, j $= \mathrm{H_2}, \mathrm{H_2O}$, cathode: i, j $= \mathrm{O_2}$, $\mathrm{N_2}$, $\mathrm{H_2O}$	
Saturation pressure	$\log_{10} P_{\mathrm{w}}^{\mathrm{sat}} = -2.18 + 2.95 \times 10^{-2} T - 9.18 \times 10^{-5} T^2 + 1.44 \times 10^{-7} T^3$	[47]

Table 2: Parametric constants in the model

Parameter	Value	Ref.
Amplification constant (β)	0.085 V$(\mathrm{cm^2 A^{-1}})^{\mathrm{k}}$	[4, 33]
Dimensionless power in the amplification term (k)	1.1	[4, 33]
Limiting current density (I_{L})	1.4 A $\mathrm{cm^{-2}}$	[4]
Lower heating value of hydrogen (LHV)	2.4×10^5 J $\mathrm{mol^{-1}}$	[25]
Oxygen exchange current density (I_0)	0.01 A $\mathrm{cm^{-2}}$	[31]
Reversible open-circuit potential (V_{oc})	1.1 V	[31]
Membrane		
Diffusion coefficient of water in membrane (D_0)	5.5×10^{-7} $\mathrm{cm^2\ s^{-1}}$	[28]
Dry density ($\rho_{\mathrm{m,dry}}$)	2.0 g $\mathrm{cm^{-3}}$	[28]
Dry equivalent weight ($M_{\mathrm{m,dry}}$)	1100 g $\mathrm{mol^{-1}}$	[28]
Thickness (t_{m})	5×10^{-3} cm (50 μm)	
Compressor		[34]
Compressor efficiency (η_{c})	0.85	
Entry air temperature (T_{e})	288 K (15 °C)	
Inlet pressure (P_{in})	1 atm	
Motor efficiency (η_{mt})	0.85	
Specific heat constant of air (c_{p})	1004 J $\mathrm{K^{-1} kg^{-1}}$	

Table 3: Comparison of the representative solutions in the Pareto set (Figure 3) with the base case at stack output power of 50 kW

	η (%)	A ($\times 10^4 \mathrm{cm}^2$)	I ($\mathrm{A\,cm}^{-2}$)	V (V)	P (atm)	$\lambda_{\mathrm{H_2}}$	λ_{air}	RH_{fuel}	RH_{air}	W_{fuel} (kW)	W_{prs} (kW)
Base case	44.18	25	0.25	0.79	2	1.25	2	1	0.5	98.52	6.47
$\omega = 1$	53.15	52.93	0.11	0.86	3.03	1.10	1.66	1	0.5	79.66	7.66
$\omega = 0.85$	51.33	40.56	0.14	0.87	4.91	1.10	1.53	1	0.5	78.44	9.74
$\omega = 0.5$	42.20	19.19	0.35	0.75	5.00	1.10	1.58	1	0.5	91.65	11.32
$\omega = 0.15$	32.41	15.00	0.56	0.60	5.00	1.10	1.46	1	0.5	114.96	12.74
$\omega = 0$	24.80	14.51	0.67	0.51	5.00	1.20	1.39	1	0.5	145.60	13.89

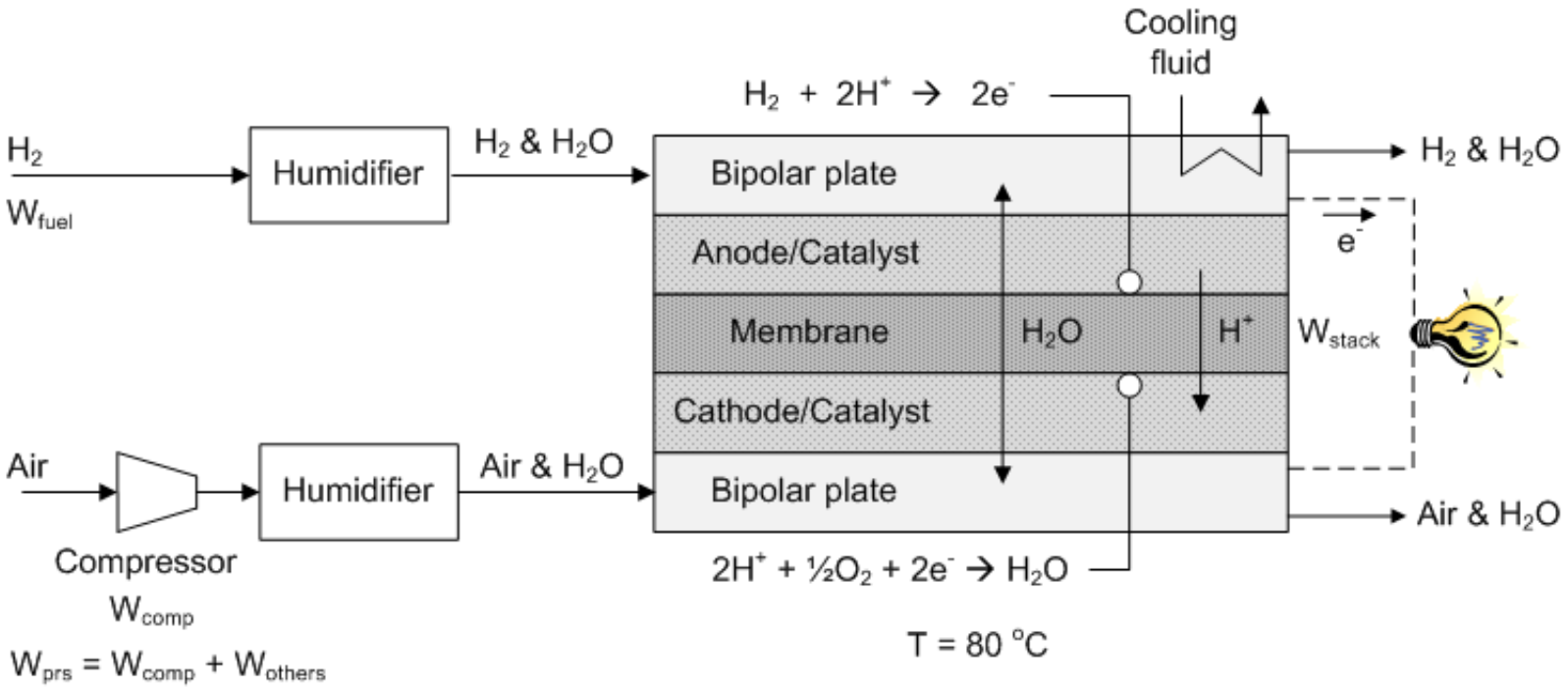

Figure 1: A general hydrogen-air PEM fuel cell system with a single-cell stack.

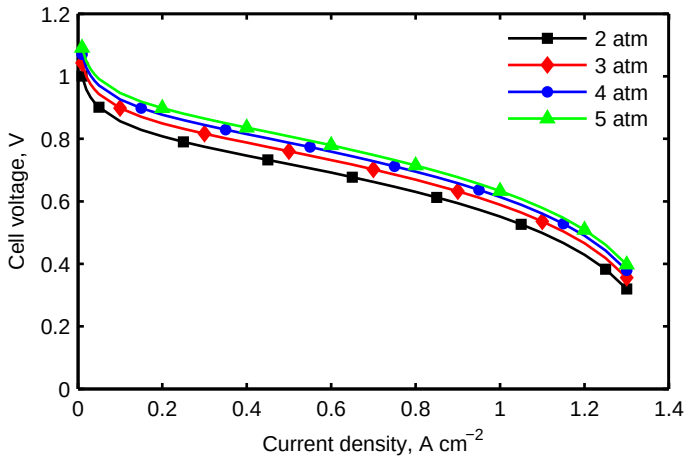

(a)

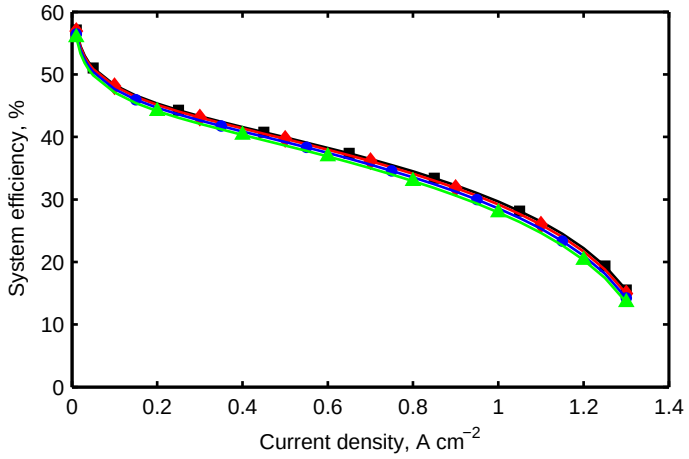

(b)

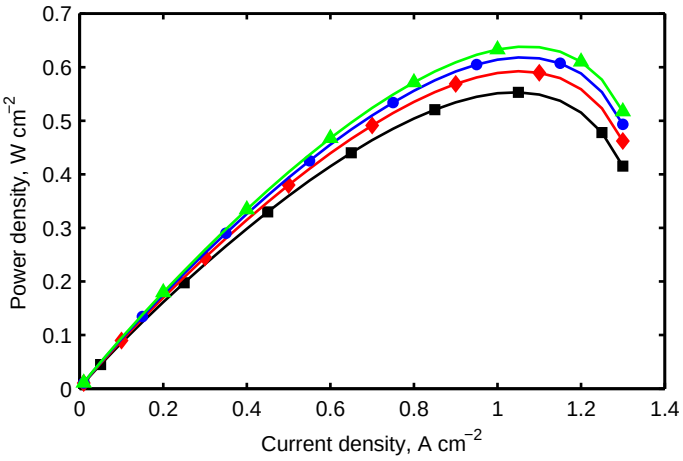

(c)

Figure 2: Simulation of the system for a base case: (a) polarisation curve, (b) system efficiency, and (c) power density, all with respect to the current density at various operating pressures.

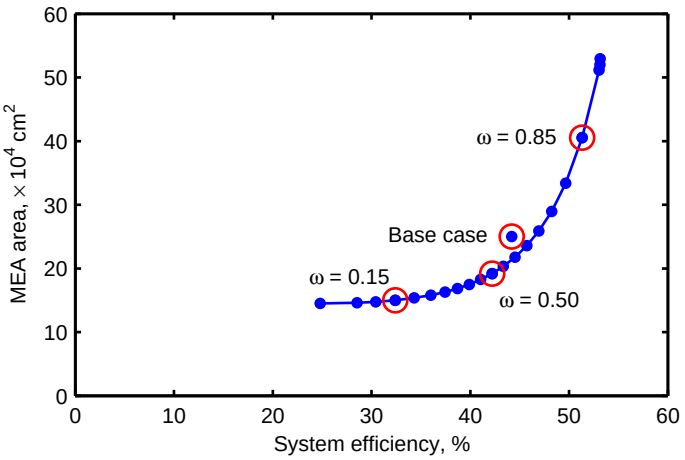

Figure 3: Pareto set at stack output power of 50 kW.

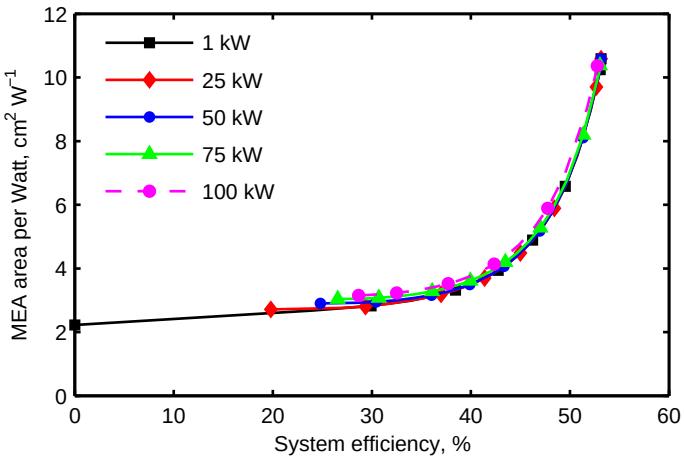

(a)

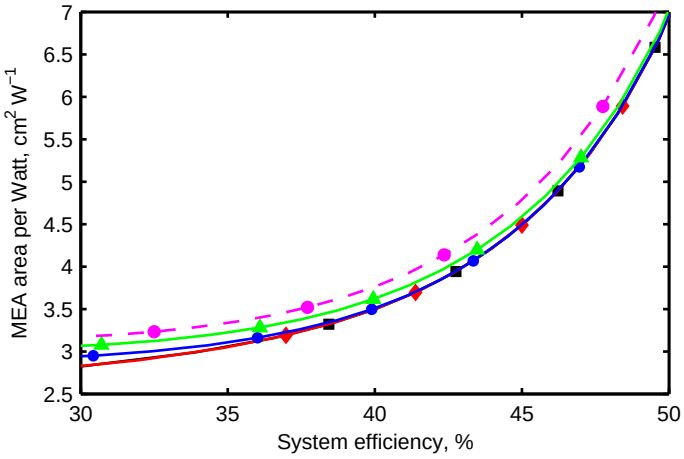

(b)

Figure 4: Comparison of the Pareto sets at different stack output power, showing (a) the entire range and (b) an enlarged region to emphasise the difference in the solutions.

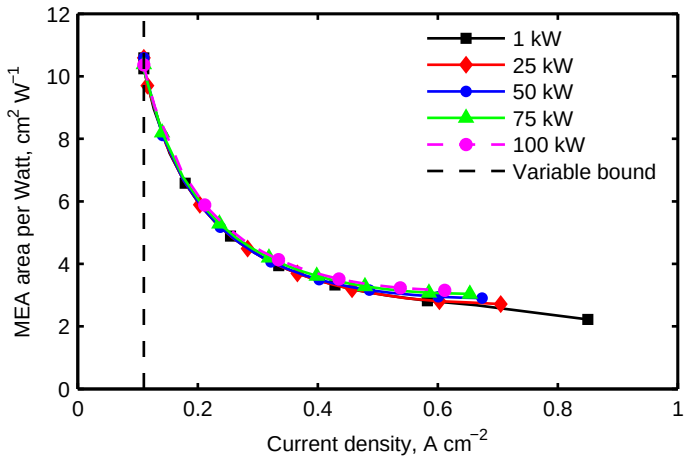

(a)

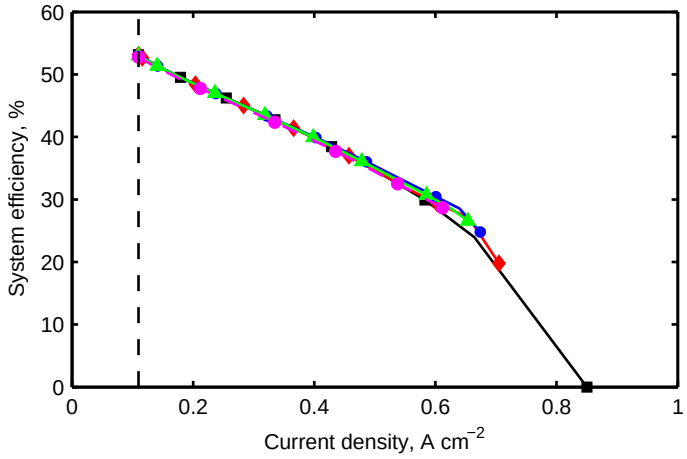

(b)

Figure 5: Optimal values of the design objectives plotted against the current density: (a) MEA area per Watt and (b) system efficiency.

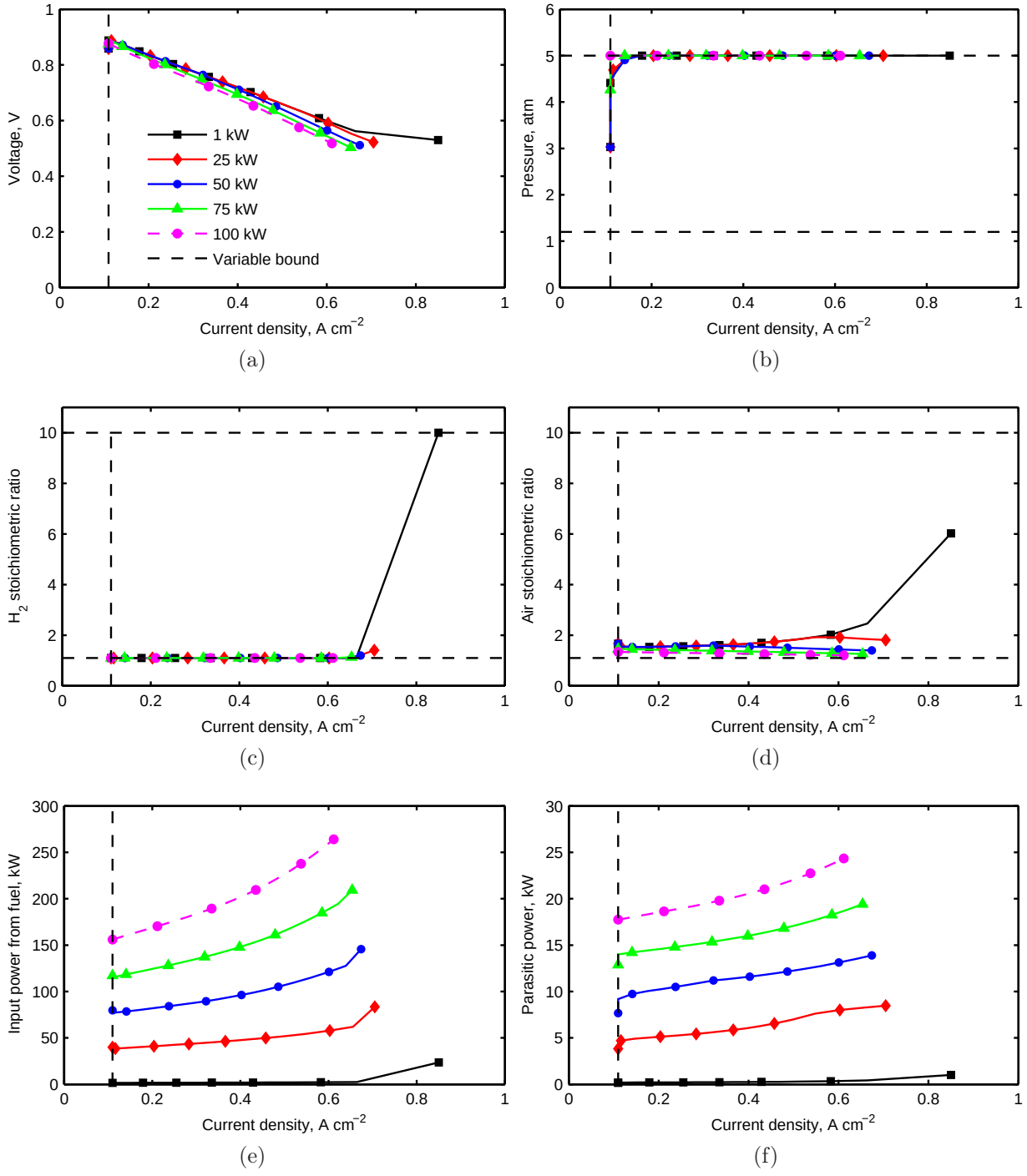

Figure 6: Optimal values of some of the design variables plotted against the current density: (a) voltage, (b) pressure, (c) hydrogen stoichiometric ratio, (d) air stoichiometric ratio, (e) input power and (f) parasitic power.

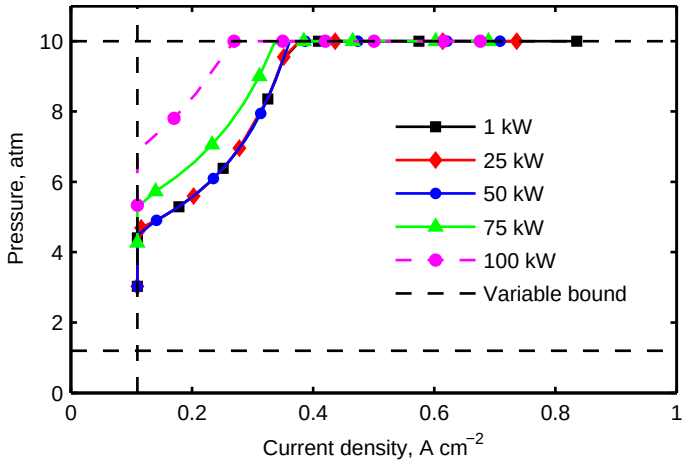

Figure 7: Optimal values of the operating pressure with the upper bound increased to 10 atm.

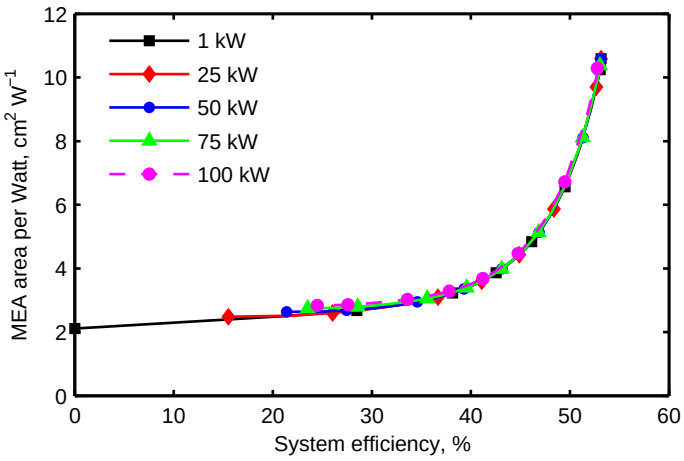

(a)

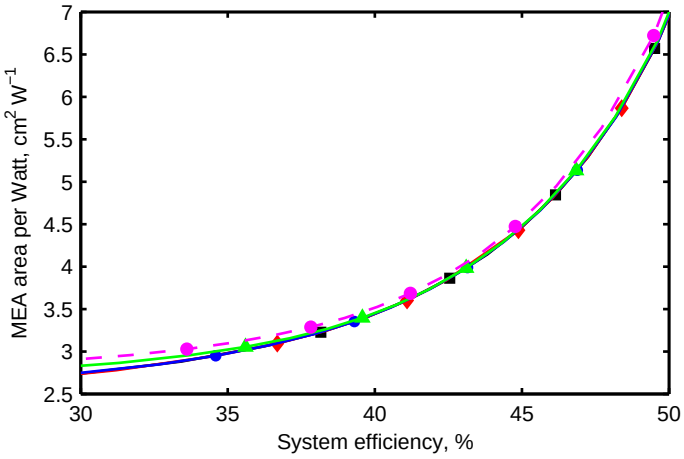

(b)

Figure 8: Comparison of the Pareto sets at different stack output power with the upper bound on the pressure increased to 10 atm, showing (a) the entire range and (b) an enlarged region to emphasise the difference in the solutions

Nomenclature

A	Total active area of the MEA , cm^2
a	Water activity
c	Concentration of water, mol cm^{-3}
c_p	Specific heat constant of air, J $K^{-1}kg^{-1}$
D_w	Diffusion coefficient of water in the membrane, cm^2 s^{-1}
D_0	A parameter used in the expression for diffusion coefficient of water, cm^2 s^{-1}
F	Faraday's constant, 96487 C eq^{-1}
f	Fraction of liquid water in the channel
I	Current density, A cm^{-2}
I_0	Exchange current density, A cm^{-2}
I_L	Limiting current density, A cm^{-2}
LHV	Lower heating value of hydrogen, 2.4×10^5 J mol^{-1}
M	Molar flow rate, mol s^{-1}
$M_{m,dry}$	Membrane dry weight, g mol^{-1}
m_{air}	Mass flow rate of air, kg s^{-1}
n_{cell}	Number of cells in a stack, (1)
n_d	Electro-osmotic coefficient (number of water molecules carried per proton)
P	System pressure, atm
P_i	Partial pressure of component i, atm
P_{in}	Inlet air pressure to the compressor
R	Gas constant, 8.314 J mol^{-1} K^{-1} or 82.057 cm^3 atm mol^{-1} K^{-1}
RH	Relative humidity
T	Temperature, °C
T_e	Entry air temperature, K
t_m	Thickness of the membrane, cm

V	Voltage, V
W	Power, W
y	Mole fraction of water vapour
z	Weighted sum of the objectives
z_i	A single objective

Greek symbols

α	Net water molecules per proton flux ratio
β	Amplification constant, V$(\mathrm{cm}^2\mathrm{A}^{-1})^{\mathrm{k}}$
η	System efficiency, %
η_{c}	Compressor connecting efficiency
η_{mt}	Motor efficiency
λ	Stoichiometric ratio
$\rho_{\mathrm{m,dry}}$	Dry membrane density, g cm^{-3}
σ_{m}	Membrane conductivity, Ohm^{-1} cm^{-1}
ω	Weighting factor

Subscript

a	Anode
c	Cathode
comp	Compressor
H_2	Hydrogen
N_2	Nitrogen
O_2	Oxygen
oc	Open circuit
prs	Parasitic

w	Water

Superscript

k	Dimensionless power in the amplification term
l	Liquid
sat	Saturated
v	Vapour